PHYSICAL REVIEW C VOLUME 3, NUMBER 2 FEBRUARY 1971

Off-Shell Effects in Nuclear Matter

Michael I. Haftel*
Naval Research Laboratory, Washington, D. C. 20390

and

Frank Tabakin
Physics Department, University of Pittsburgh, Pittsburgh, Pennsylvania 15213
(Received 5 November 1970)

We examine the binding energy of nuclear matter for exactly phase-shift-equivalent potentials. We generate these potentials by applying a short-range unitary transformation to the Reid soft-core potential. All potentials have a one-pion-exchange tail. We find that, for the potentials studied, variations of up to 9.5 MeV in the binding energy and 0.33 F^{-1} in the saturation density occur. The variations in binding energy are linearly correlated with the wound integral κ for those potentials that give nearly the same deuteron electric form factor. An increase in κ leads to less binding in nuclear matter. The sensitivity of the binding energy is somewhat greater to the $^3S_1+^3D_1$ contribution to κ than to the $^1S_0$ contribution to κ. We give a theoretical explanation, based on the modified Moszkowski-Scott separation approximation, to account for the sensitivity of the binding energy to the $^1S_0$ and $^3S_1+^3D_1$ contributions to κ. We also discuss the relation of κ and the binding energy of nuclear matter to the off-shell elements of the T matrix. We discover that far-off-shell elements ($q \gtrsim 6$ F^{-1}) play a significant role in nuclear matter.

I. INTRODUCTION

The two-nucleon elastic scattering data and certain bound-state properties provide the only direct experimental criteria one can apply to the two-nucleon interaction. The scattering data only fix the asymptotic form of the two-nucleon wave function; the wave function at short distances, aside from meson-theoretic constraints,[1-4] is undetermined. Equivalently, the scattering data determine the on-energy-shell matrix elements of the transition (T) matrix; the off-energy-shell T matrix is undetermined by the two-nucleon data. The question arises—how sensitive are the properties of three- and more-nucleon systems to the short-range part of the two-nucleon wave function or to the off-energy-shell T matrix? This paper considers this question for infinite nuclear matter. The investigation of off-shell effects in nuclear matter is especially important in view of the disagreement between the binding energies obtained from "realistic" local potentials (10 to 11 MeV/A)[5-8] and the semiempirical mass formula prediction of 16 MeV/A.

Recently a number of investigators have studied off-shell effects in proton-proton bremsstrahlung.[9,10] The results of these studies indicate only small off-energy-shell effects. Investigations into the off-shell effects in the three-nucleon bound-state problem are still in the preliminary stages.[11,12] On the other hand, several investigators[7,13,14] have suggested that off-shell effects in nuclear matter are definitely very important.

In a previous paper[7] the present authors reported variations of up to 20 MeV per particle in the binding energy of nuclear matter for potentials that give nearly the same fits to the two-body data. These variations were principally attributable to drastic off-shell alterations in the tensor force. Coester *et al.*[14] found similar variations in the S-wave potential energy contribution in nuclear matter for exactly phase-shift-equivalent potentials.

This paper investigates, in detail, the binding energy of nuclear matter for exactly phase-shift-equivalent potentials. The potentials we consider are generated from the Reid soft-core potential[15] by a special case of the rank-two unitary transformation described by Coester and co-workers.[14] Our potentials differ from those in Ref. 14 insofar as we start with a potential that fits the experimental two-body data. Also, we transform the wave functions in the coupled $^3S_1+^3D_1$ state as well as the uncoupled $^1S_0$ state. For the $^3S_1+^3D_1$ state we classify our potentials according to their deuteron electric quadrupole moments and electric form factors. All potentials have the required one-pion-exchange (OPE) tail. Furthermore, the wave functions of the potentials studied differ mainly inside a distance of 1 F. Within this distance (1 F) the ambiguity concerning the two-nucleon wave function arises from both experimental and meson-theoretic considerations.[1-4]

Two goals motivate our study. First, we wish to determine how important off-shell effects are in nuclear matter. Second, we wish to discover how variations in binding energy are related to off-shell matrix elements. Several workers[7,14,16] have

suggested that the binding energy of nuclear matter is related to the "wound" integral κ.[17,18] We study the κ dependence of the binding energy of nuclear matter in Sec. III of this paper. We find that the binding energy, at a fixed density, is a linear function of κ. In Sec. IV we discuss the theoretical foundation of this linear relation on the basis of the modified Moszkowski-Scott (MMS) separation approximation.[19] In Sec. V we discuss the sensitivity of nuclear matter results to the off-shell T matrix. We concentrate on the relation of κ to the "half-shell" T matrix, which is determined by the two-nucleon scattering wave functions.[20] Our conclusion is that the binding energy of nuclear matter is sensitive to a large region of the half-shell T matrix. Far-off-shell effects are important. In Sec. VI we summarize our results and suggest how nuclear matter can be used to help pin down the two-nucleon interaction.

Before we present the results of our nuclear matter calculations, we describe our phase-shift-equivalent potentials. We also briefly discuss our solution to the Brueckner equation. To these two topics we devote Sec. II.

II. PHASE-SHIFT-EQUIVALENT POTENTIALS AND THE SOLUTION OF THE BRUECKNER EQUATION

Phase-shift-equivalent potentials may be generated by the application of a short-range unitary operator U to the two-nucleon scattering solutions to the Schrödinger equation,[14,21,22] i.e.,

$$\tilde{\Psi}^+(\vec{r}) = U\Psi^+(\vec{r}) \quad \text{and} \quad \tilde{\Psi}^+(\vec{r}) \underset{r\to\infty}{\longrightarrow} \Psi^+(\vec{r}) . \tag{1}$$

If we consider the special case, $U = 1 - 2\Lambda$, where Λ is a Hermitian operator, the requirement of unitarity reduces to

$$\Lambda^2 = \Lambda , \tag{2}$$

i.e., Λ is a projection operator. If we further require that $\langle\vec{r}|\Lambda|\vec{r}'\rangle \underset{r\to\infty}{\longrightarrow} 0$ faster than $1/r$, then the scattering solutions $\tilde{\Psi}^+(\vec{r})$ give the same scattering cross sections and phase shifts as $\Psi^+(\vec{r})$. Since U is unitary, orthonormality and completeness of states is assured. Also, the eigenvalues of the two-body system remain invariant under the transformation U.

To relate U with phase-shift-equivalent potentials, we consider a Hamiltonian $H = T + V$, where T is the kinetic energy and V the potential energy. The transformed Hamiltonian ($\tilde{H}$) becomes

$$\tilde{H} = U^\dagger H U . \tag{3}$$

If Ψ is a solution to $H\Psi = E\Psi$, then $\tilde{\Psi}$ is a solution to $\tilde{H}\tilde{\Psi} = E\tilde{\Psi}$. The transformed Hamiltonian (3) may be written

$$\tilde{H} = T + V - 2\Lambda V - 2V\Lambda + 4\Lambda V\Lambda - 2\Lambda T - 2T\Lambda + 4\Lambda T\Lambda . \tag{4}$$

We define a "transformed" potential $\tilde{V}$ by

$$\tilde{H} \equiv T + \tilde{V} . \tag{5}$$

The transformed potential $\tilde{V}$ is given by

$$\tilde{V} = V - 2\Lambda V - 2V\Lambda + 4\Lambda V\Lambda - 2\Lambda T - 2T\Lambda + 4\Lambda T\Lambda . \tag{6}$$

The transformed potential, $\tilde{V}$, if substituted into the Schrödinger equation, gives the same two-body cross sections and two-body eigenvalues as V. The transformed potential $\tilde{V}$, however, does not correspond to a unitary transformation of the wave function for a many-body system; therefore, we should not expect V and $\tilde{V}$ to give the same energy spectrum in finite nuclei or infinite nuclear matter.

In this paper we choose $\langle\vec{r}|\Lambda|\vec{r}'\rangle$ to have the partial-wave decomposition

$$\langle\vec{r}|\Lambda|\vec{r}'\rangle = \sum_{LL'\alpha MT_3} g_L^\alpha(r) g_{L'}^\alpha(r') \mathcal{Y}_L^{\alpha MT_3}(\hat{r}) \mathcal{Y}_L^{\alpha MT_3\dagger}(\hat{r}') A_{LL'}^\alpha . \tag{7}$$

The quantum numbers L and L' refer to orbital angular momentum, α refers to the quantum numbers J (total angular momentum), S (spin), and T (isospin), while M and T_3 are the projections of J and T. The $\mathcal{Y}_L^{\alpha MT_3}$ are normalized eigenfunctions of the indicated quantum numbers. The form (7) is not the most general choice of Λ. The choice (7), however, retains all of the required symmetries of the N-N interaction [providing $g_L^\alpha(r)$ is real], and is particularly convenient for numerical calculations.

Unitarity requires that $g_L^\alpha(r)$ be square integrable. If we normalize all the g_L^α to unity, the unitarity requirement (2) becomes

$$A_{LL} = 1 \quad \text{for uncoupled channels,}$$

and

$$A_{LL'}^\alpha = \delta_{LL'} \quad \text{or} \quad \begin{matrix} \\ J-1 \\ J+1 \end{matrix} \begin{pmatrix} \overset{J-1}{\sin^2\theta} & \overset{J+1}{\sin\theta\cos\theta} \\ \sin\theta\cos\theta & \cos^2\theta \end{pmatrix} \tag{8}$$

for coupled channels. The parameter θ in Eq. (8) is real but otherwise arbitrary.

The operator Λ defined by Eq. (7) is a projection operator onto the space spanned by the states $g_L^\alpha \mathcal{Y}_L^{\alpha MT_3}$ for $A_{LL'} = \delta_{LL'}$, or onto $\sin\theta g_{J-1}^\alpha \mathcal{Y}_{J-1}^{\alpha MT_3} + \cos\theta g_{J+1}^\alpha \mathcal{Y}_{J+1}^{\alpha MT_3}$. The operator Λ has a separable form in either configuration or momentum space.

In momentum space

$$\langle\vec{k}|\Lambda|\vec{k}'\rangle = \frac{2\hbar^2}{\pi M} \sum_{LL'\alpha MT_3} i^{(L'-L)} g_L^\alpha(k) g_{L'}^\alpha(k') \times \mathcal{Y}_L^{\alpha MT_3}(\hat{k}) \mathcal{Y}_{L'}^{\alpha MT_3\dagger}(\hat{k}') A_{LL'}^\alpha ,$$

where $g_L^\alpha(k) = \int_0^\infty r^2 dr\, g_L^\alpha(r) j_L(kr)$. While Λ is separable and, in the case where V is the Reid potential, V is local; $\tilde{V}$, by Eq. (6), is neither local nor separable. Therefore solution of the Brueckner equation[23] in the momentum space provides the most convenient method of calculating the G matrix in nuclear matter.

The solution of the Brueckner equation in momentum space is given in detail in Ref. 7. To solve the Brueckner equation we write the Brueckner G matrix in terms of its partial-wave contributions

$$\langle \vec{k}|G(\omega)|\vec{k}'\rangle = \frac{2\hbar^2}{\pi M} \sum_{LL'\alpha MT_3} i^{L'-L} G^\alpha_{LL'}(k,k',\omega) \times \mathcal{Y}_L^{\alpha MT_3}(\hat{k}) \mathcal{Y}_{L'}^{\alpha MT_3\dagger}(\hat{k}') . \quad (9)$$

The G matrix thereupon is a solution to the partial-wave Brueckner equation[7,23]

$$G^\alpha_{LL'}(k,k',\omega) = V^\alpha_{LL'}(k,k') + \frac{2}{\pi} \sum_l \int_0^\infty q^2 dq\, V^\alpha_{Ll}(k,q) \times \frac{Q}{\omega - q^2} G^\alpha_{lL'}(q,k',\omega) . \quad (10)$$

The V-matrix elements and the normalization used in Eq. (10) are given in Ref. 7. The Pauli Q operator projects out occupied states, and ω is determined from the self-consistent single-particle energies given by the prescription in Ref. 19 by Bethe, Brandow, and Petschek (BBP). In Eq. (10) we have employed the usual angle average and effective mass approximations in which $Q/(\omega - q^2)$ depends only on q, k', and the magnitude of the center-of-mass momentum (K). We have also assumed a free-particle spectrum for unoccupied states. We solve the one-dimensional integral Eq. (10) by replacing the infinite integral by a finite summation. We solve the resulting linear equations by matrix inversion.

The binding energy per particle (E) of nuclear matter, in the Brueckner approximation, is given by

$$E = \frac{3\hbar^2 k_F^2}{10M} + \frac{4\hbar^2}{\pi M} \sum_{L\alpha} (2J+1)(2T+1) \times \int_0^{k_F} k_0^2 dk_0 \left(1 - \frac{3}{2}\frac{k_0}{k_F} + \frac{1}{2}\frac{k_0^3}{k_F^3}\right) G^\alpha_{LL}(k_0,k_0,\omega) . \quad (11)$$

In determining the values of ω to be inserted into Eq. (11), we assume that the center-of-mass momentum is given by an "average" center-of-mass momentum. For two particles in the Fermi sea with relative momentum k_0, this average center-of-mass momentum is given by[24]

$$K_{av} = \tfrac{3}{5} k_F^2 \left(1 - \frac{k_0}{k_F}\right)\left(1 + \frac{k_0^2/k_F^2}{3(2 + k_0/k_F)}\right) . \quad (12)$$

According to Eq. (10), the essential input information necessary to calculate G and E are the matrix elements of V in momentum space. The matrix elements of the Reid soft-core potential have been accurately calculated previously.[7] The separable form of Λ allows the rapid evaluation of the matrix elements of $\tilde{V}$.

We have calculated G and E for various potentials $\tilde{V}$. The G matrices ($\tilde{G}$) were calculated for values of ω corresponding to the self-consistent single-particle energies for the Reid soft-core potential with all partial waves.[7] The binding energies so obtained were then corrected for self-consistency by a method we describe in Sec. IV. We now present the results of our calculations.

III. RESULTS AND DISCUSSION

In employing the transformation (7) we choose

$$g_0^\alpha(r) = C_0 e^{-\alpha_0 r}(1 - \beta_0 r) \quad (13)$$

for the $^1S_0$ state, and

$$g_0^\alpha(r) = C_0 e^{-\alpha_0 r}(1 - \beta_0 r), \quad g_2^\alpha(r) = C_2 r\, e^{-\alpha_2 r}(1 - \beta_2 r) \quad (14)$$

for the $^3S_1 + {}^3D_1$ state. We also consider the case

$$g_2^\alpha(r) = C_2' r^2 e^{-\alpha_2' r}(1 - \beta_2' r) \quad (15)$$

for the $^3S_1 + {}^3D_1$ state. The C_L's are determined from the normalization requirement $\int_0^\infty r^2 dr\, |g_L^\alpha(r)|^2 = 1$. In Eqs. (13)–(15), g_0 transforms the $L=0$ component of the wave function, while g_2 transforms the $L=2$ component.

In the transformations (13)–(15), $g_L^\alpha(r)$ approaches zero more rapidly than $e^{-\mu r}/r$ as long as $\alpha_L > \mu$. Therefore, as long as α_L is greater than the pion mass (about $\mu = 0.70$ F^{-1}) the transformed potential $\tilde{V}$ is asymptotically local and has an OPE tail, providing that V has these properties. Table I lists the parameters α_0 and β_0 for the transformed Reid soft-core $^1S_0$ potential. In Table II we list the parameters α_0, β_0, α_2, β_2, α_2', β_2', and θ for the $^3S_1 + {}^3D_1$ transformations. Note that, in all cas-

TABLE I. Parameters used for transformed $^1S_0$ potentials.

Potential	α_0 (F^{-1})	β_0 (F^{-1})
R (Reid)	...	...
1	3.00	1.20
2	4.00	1.60
3	3.00	1.00
4	4.00	1.00
5	4.00	1.04
6	3.00	0.90
7	3.00	0.95

TABLE II. Parameters used for transformed $^3S_1+^3D_1$ potentials.

Potential	α_0 (F^{-1})	β_0 (F^{-1})	α_2 (F^{-1})	β_2 (F^{-1})	α_2' (F^{-1})	β_2' (F^{-1})	$\sin\theta$
R (Reid)	•••	•••	•••	•••	•••	•••	•••
8	2.40	0.80	•••	•••	•••	•••	1
9	•••	•••	3.00	0.83	•••	•••	0
10	•••	•••	3.00	0.85	•••	•••	0
11	•••	•••	2.40	0.72	•••	•••	0
12	•••	•••	3.60	0.93	•••	•••	0
13	•••	•••	3.60	1.00	•••	•••	0
14	•••	•••	3.60	0.90	•••	•••	0
15	•••	•••	3.00	0.78	•••	•••	0
16	4.33	1.25	•••	•••	•••	•••	1
17	•••	•••	•••	•••	3.50	0.80	0
18	4.00	1.30	•••	•••	•••	•••	1
19	2.40	0.83	•••	•••	•••	•••	1
20	2.70	0.88	•••	•••	•••	•••	1
21	2.70	0.91	•••	•••	•••	•••	1
22	2.20	0.80	•••	•••	•••	•••	1
23	3.00	1.20	•••	•••	•••	•••	1
24	•••	•••	•••	•••	3.50	0.50	0
25	•••	•••	•••	•••	3.50	0.00	0
26	•••	•••	•••	•••	4.20	0.00	0

TABLE III. Bound-state observables for potentials 8–26 and the Reid potential. Potentials that do not give the same electric form factor as the Reid potential, to within experimental error, are marked with x.

			$(N_B \equiv [\langle\tilde{\Psi}-\Psi_{\text{Reid}}\|\tilde{\Psi}-\Psi_{\text{Reid}}\rangle]^{1/2})$							
	P_D	Q	$100F_{e1}^2(q^2)/(G_{Ep}+G_{En})^{2\,a}$							
Potential	(%)	(F^2)	$q^2=1.0$	3.0	6.0	9.0	12.0	16.07	24.25	N_B
R (Reid)	6.47	0.282	37.88	11.20	3.198	1.268	0.6446	0.3569	0.1982	•••
8	6.47	0.282	37.81	11.12	3.131	1.227	0.6229	0.3504	0.2017	0.0054
9	6.47	0.281	37.89	11.21	3.203	1.270	0.6448	0.3560	0.1974	0.0138
10	6.47	0.279	37.93	11.25	3.227	1.279	0.6451	0.3512	0.1923	0.0316
11	6.47	0.282	37.87	11.19	3.188	1.263	0.6430	0.3564	0.1972	0.0012
12	6.47	0.281	37.89	11.22	3.204	1.270	0.6445	0.3552	0.1962	0.0172
13	6.47	0.278	37.95	11.29	3.251	1.287	0.6418	0.3328	0.1731	0.0610
14	6.47	0.282	37.88	11.20	3.191	1.265	0.6445	0.3586	0.2001	0.0004
15	6.47	0.284	37.83	11.15	3.163	1.253	0.6402	0.3574	0.1961	0.0282
16	6.47	0.282	37.90	11.24	3.221	1.284	0.6542	0.3595	0.1936	0.0282
17	6.47	0.278	37.94	11.27	3.231	1.280	0.6451	0.3511	0.1939	0.0296
18	6.47	0.282	38.01	11.36	3.323	1.354	0.6969	0.3749	0.1810	0.0804
19	6.47	0.282	38.01	11.35	3.302	1.332	0.6799	0.3689	0.1933	0.0364
20	6.47	0.282	37.93	11.25	3.226	1.285	0.6539	0.3599	0.1966	0.0200
21	6.47	0.282	38.04	11.39	3.341	1.359	0.6968	0.3751	0.1891	0.0524
22 x	6.47	0.281	38.16	11.57	3.467	1.434	0.7388	0.3920	0.1903	0.0606
23 x	6.47	0.277	38.96	12.74	4.557	2.319	1.434	0.8958	0.4923	0.2586
24 x	6.47	0.274	37.94	11.25	3.160	1.149	0.4695	0.1451	0.0057	0.2402
25 x	6.47	0.234	38.26	11.56	3.269	1.163	0.4714	0.1894	0.1513	0.3618
26 x	6.47	0.259	38.13	11.46	3.264	1.180	0.4663	0.1328	0.0170	0.2912
Approximate experimental error (%) [b]		1%	5%	6%	8%	10%	10%	10%	25%	

[a] G_{Ep} and G_{En} are the proton and neutron form factors, respectively.
[b] Approximate experimental errors are for $F_{e1}(q^2)$ and are taken from Ref. 26 and references listed therein.

es, $\alpha_L > \mu$; therefore, all of the transformed potentials represented in Tables I and II have local OPE tails. Since $\alpha_L \geq 2.2$ F^{-1} in all cases, the transformations in Tables I and II leave the wave functions past 1 F relatively unaffected. Meson theory[1-4] leaves the wave function arbitrary at distances within about 1 F. Therefore, the potentials represented in Tables I and II, along with the Reid potential, are equivalent on the basis of the two-body data and meson theory.

We also classify the potentials in Table II according to the electric quadrupole moments (Q) and electric form factors $[F_{el}(q^2)]$ they yield.[25] Table III lists the bound-state observables for the potentials in Table II. We use the approximate experimental errors,[26] listed on the last line in Table III, as the basis for classification. Those potentials (22–26) that do not give the same electric form factor as the Reid potential, to within experimental error,[27] are marked with an "x" in Table III. We notice that all the potentials with approximately the same form factor (potentials 8–21) also have approximately the same electric quadrupole moment (to within 0.004 F^2). Since we desired that all of the potentials give the same D-state probability, we chose $\sin\theta = 0$ or 1. These choices of $\sin\theta$ leave the S- and D-wave norms individually invariant.[28]

The question now arises—given a set of potentials that are equivalent on the basis of the two-body bound-state and scattering data, what variations in nuclear binding energies may we expect? We answer this question by Figs. 1 and 2. In Fig. 1 we give the saturation curves for several of the cases in Table I. In Fig. 2 we give the saturation curves for several of the cases in Table II. In Fig. 2 we also give an example of a saturation curve (1+11) for a transformation that alters both the $^1S_0$ and $^3S_1+{}^3D_1$ wave functions. In Fig. 1 we find variations up to about 6.5 MeV in the saturation energy and 0.17 F^{-1} in the saturation Fermi momentum (k_F). Variations up to 6.3 MeV in the saturation energy and 0.29 F^{-1} in the saturation Fermi momentum occur for the cases where the $^3S_1+{}^3D_1$ potential is transformed in Fig. 2. If we include the combination of transformation 1 in the $^1S_0$ case with transformation 11 in the $^3S_1+{}^3D_1$ state, as in curve 1+11, a 9.5-MeV variation in binding energy and a 0.33-F^{-1} variation in saturation Fermi momentum occurs.

Two interesting patterns manifest themselves in Figs. 1 and 2. First, variations in energy at a given density are greater at higher densities. For instance, the maximum variation in energy at k_F

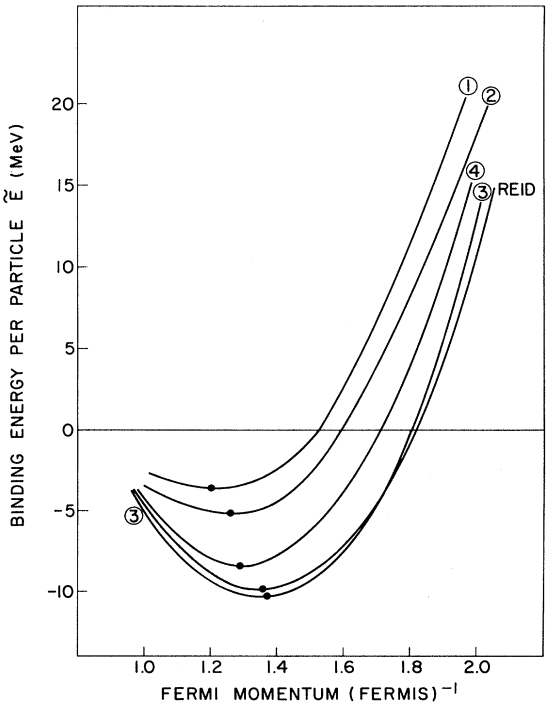

FIG. 1. The saturation curves for several $^1S_0$ transformed potentials. The heavy dots indicate the saturation minima.

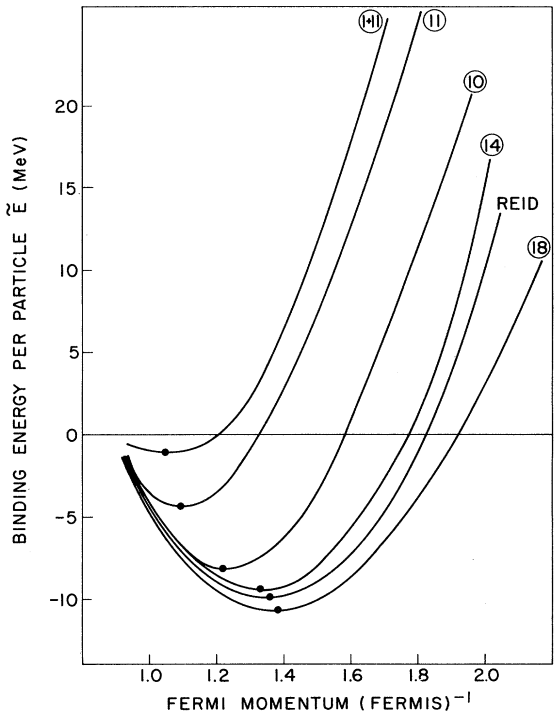

FIG. 2. The saturation curves for several $^3S_1+{}^3D_1$ transformed potentials. Curve 1+11 combines transformed potential 1 in the $^1S_0$ state and transformed potential 11 in the $^3S_1+{}^3D_1$ state. The heavy dots indicate the saturation minima.

$= 1.1\ \mathrm{F}^{-1}$ is about 6.6 MeV; at $k_F = 1.4\ \mathrm{F}^{-1}$ (approximately the empirical saturation density) the maximum variation is about 17 MeV; at $k_F = 1.7\ \mathrm{F}^{-1}$, the variation increases to about 29 MeV. Second, potentials with larger binding energies give greater saturation densities. This second characteristic is, no doubt, a consequence of the first. The reasons for the density dependence of the saturation curves in Figs. 1 and 2 will become evident in our later discussion.

The saturation curves in Figs. 1 and 2 indicate that off-energy-shell effects are important in the Brueckner theory of nuclear matter. The variation in binding energy observed is greater than the current 5- to 6-MeV disagreement between the binding energies of "realistic" local potentials (e.g., Reid) and the binding energy predicted by the semiempirical mass formula (16 MeV). Furthermore, the variation is probably greater than the contribution attributable to the "three-body diagrams" (1–3 MeV)[29,30] for "realistic" potentials. We now investigate how these off-energy-shell variations are correlated.

Several authors[7,14,16] have suggested that the binding energy of nuclear matter is related to the "wound integral" κ, where κ is defined[17]

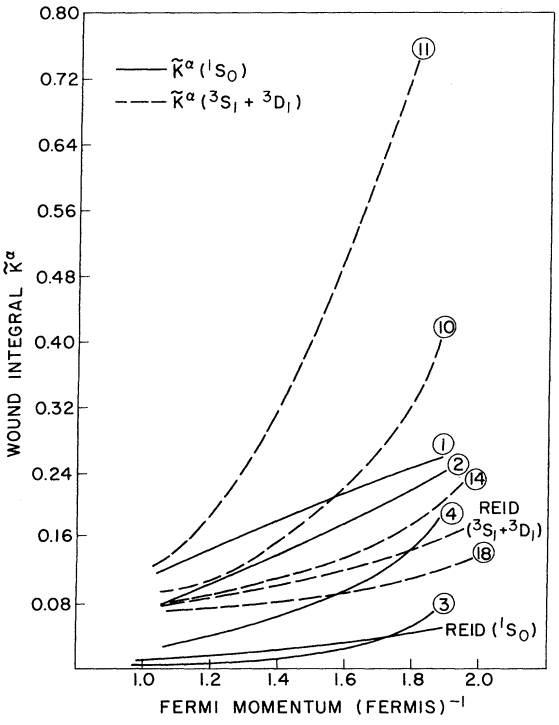

FIG. 3. The $^1S_0$ and $^3S_1+{}^3D_1$ contributions to the wound integral $\tilde{\kappa}^\alpha$ for the potentials used in Figs. 1 and 2. The solid lines represent the $^1S_0$ contributions as functions of density. The broken lines represent the $^3S_1+{}^3D_1$ contributions as functions of density.

$$\kappa = (2\pi)^3 \rho \langle \xi_{\mu\nu} | \xi_{\mu\nu} - \xi_{\nu\mu} \rangle . \tag{16}$$

The defect wave function $\xi_{\mu\nu}$ is simply given by $\xi_{\mu\nu} = \Phi_{\mu\nu} - \Psi^N_{\mu\nu}$. The wave function $\Phi_{\mu\nu}$ is a δ-function normalized plane wave for two particles (μ and ν) in the Fermi sea, and $\Psi^N_{\mu\nu}$ is the correlated nuclear wave function for two particles in the Fermi sea. Because of the so-called "healing" property, $\xi_{\mu\nu}(\vec{r})$ asymptotically vanishes. Therefore, κ is a measure of the "wound" or "healing distance" of the two-nucleon wave function in nuclear matter. The wound integral κ is a particularly important quantity because its average value is essentially the expansion parameter of the many-body cluster expansions[17,18,29] of the Goldstone series[31] for the ground-state energy.

In Fig. 3 we illustrate, as functions of k_F, the $^1S_0$ contributions to κ for the potentials in Fig. 1. (All wound integrals referred to in this paper represent average values of κ for two particles in the Fermi sea.) We also illustrate in Fig. 3 the $^3S_1 + {}^3D_1$ contribution to κ for the cases in Fig. 2. We notice that potentials with larger wound integrals give greater repulsion in nuclear matter. We also observe that κ is an increasing function of density. (This property results from the definition of κ [16] which includes a factor ρ.) Previous investigators[7,14,16] have noted the aforementioned relation between the binding energy of nuclear matter and κ. We now proceed to study this relation quantitatively.

In Fig. 4 we present a plot of the $^1S_0$ potential energies in nuclear matter versus the $^1S_0$ contributions to the wound integrals (κ^0_{00} of Ref. 7) for the potentials in Table I. Figure 5 is a similar

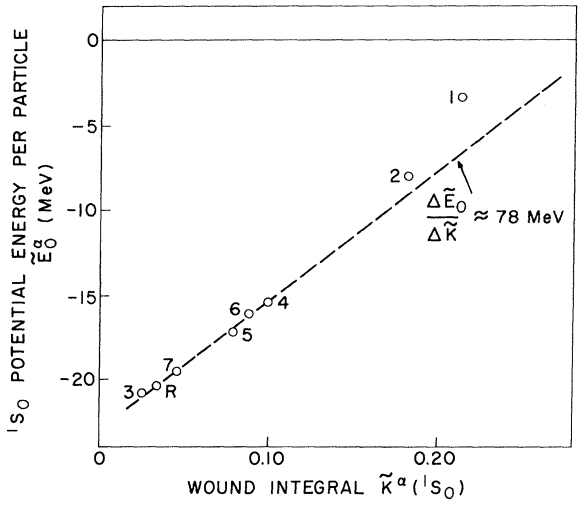

FIG. 4. The $^1S_0$ potential energies $\tilde{E}^\alpha_0$ versus the $^1S_0$ wound integrals $\tilde{\kappa}^\alpha$. The dashed line indicates the approximate linear relation between $\tilde{E}^\alpha_0$ and $\tilde{\kappa}^\alpha_0$.

plot for the $^3S_1+^3D_1$ state for the potentials in Table II, where $\kappa^\alpha = \kappa^\alpha_{00}+\kappa^\alpha_{02}+\kappa^\alpha_{20}+\kappa^\alpha_{22}$ of Ref. 7. For both Figs. 4 and 5, the Fermi momentum is $k_F = 1.6\ \mathrm{F}^{-1}$. The G matrices are calculated with starting energies (ω) determined from the self-consistent single-particle energies for the Reid potential. Accordingly, we denote the energies as $\tilde{E}_0$ to differentiate them from the self-consistent binding energies ($\tilde{E}$).

Figure 4 indicates a nearly linear dependence of $\tilde{E}_0$ on κ for the $^1S_0$ state. This linear dependence holds very well for $\tilde{\kappa}^\alpha \lesssim 3\kappa^\alpha_{\mathrm{Reid}}$. The dotted line in Fig. 4 indicates a slope of $\Delta\tilde{E}^\alpha_0/\Delta\tilde{\kappa}^\alpha \approx 78$ MeV. For larger values of κ, as in potentials 1 and 2, the slope becomes somewhat greater.

If we examine Fig. 5, we note that, again, for most of the cases in Table II, $\tilde{E}_0$ is nearly linear in κ. The slope $(\Delta\tilde{E}^\alpha_0/\Delta\tilde{\kappa}^\alpha)$ is 103 MeV compared to 78 MeV in the $^1S_0$ case. The $^3S_1+^3D_1$ potential energies are more sensitive to changes in κ than the $^1S_0$ potential energies. Disturbingly, a few potentials fall several MeV from the dotted line in Fig. 5. However, if we examine Table III, we find that, for each potential that deviates from the linear pattern, the deuteron electric quadrupole moment and/or the electric form factor deviate significantly from the Reid values. Since these potentials can be distinguished from the others on the basis of two-body bound-state observables, they should be rejected from our study. Accordingly, they appear as ×'s in Fig. 5. The conclusion here is that, for a fixed density, $\tilde{E}_0$ is linear in $\tilde{\kappa}$ for potentials that give the same two-body elastic scattering *and* bound-state observables.

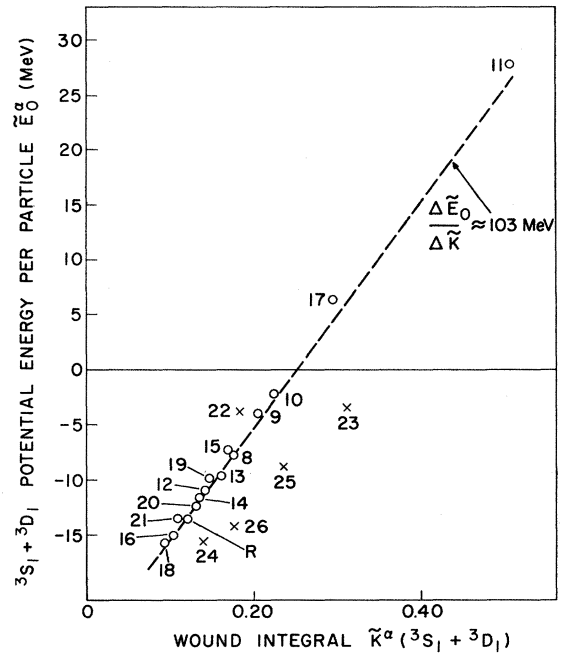

FIG. 5. The $^3S_1+^3D_1$ potential energies $\tilde{E}^\alpha_0$ versus the $^3S_1+^3D_1$ wound integrals $\tilde{\kappa}^\alpha$. Potentials marked with × do not give the same electric form factors, to within experimental error, as the Reid potential. The dashed line indicates the approximate linear relation between $\tilde{E}^\alpha_0$ and $\tilde{\kappa}^\alpha$.

Another interesting feature shown in Table III and Fig. 5 is that potentials with nearly the same deuteron wave functions may give widely varying energies in nuclear matter. To show this, we list in Table III the "difference norm," defined by $N_B = [\langle\tilde{\Psi}_B-\Psi_B|\tilde{\Psi}_B-\Psi_B\rangle]^{1/2}$, as a measure of the difference of the transformed ($\tilde{\Psi}_B$) and untransformed (Ψ_B) deuteron wave functions. We see from Table III and Fig. 5 that some potentials with very small difference norms (e.g., potentials 9, 11, and 14) give very large variations in binding energy (up to 40 MeV in $\tilde{E}_0$ at $k_F = 1.6\ \mathrm{F}^{-1}$). Also, potentials with larger difference norms generally deviate more from the dotted line in Fig. 5 than those with smaller difference norms. Henceforth in this paper, we will deal only with potentials that cannot be easily distinguished on the basis of two-body observables (e.g., potentials 1–21).

We have seen that potentials that give exactly the same two-body scattering data and nearly the same deuteron properties may give large variations (up to 9.5 MeV) in binding-energy results for nuclear matter. The binding energy of nuclear matter for these potentials is nearly linear in κ, with an increase in repulsion being associated with larger κ. We now describe a theoretical justification of this result.

IV. THEORETICAL EXPLANATION, EVALUATION, AND EXTENSION OF RESULTS

In their study of local and velocity-dependent potentials, Preston and Bhaduri[16] concluded that potentials that give the same wound integral, κ, should give about the same binding energies in nuclear matter. Coester *et al.*[14] suggested that the saturation curves for phase-shift equivalent potentials form essentially a one-parameter group. This one parameter, I in Ref. 14, we shall see shortly, is closely related to κ. Both Preston and Bhaduri, and Coester *et al.* base their arguments on the separation approximation.[19,32] We shall base our explanation on the MMS separation approximation.[19] Our discussion is based on Sec. 10 of BBP. Our arguments resemble the arguments given by Coester *et al.*[14] We evaluate and extend these arguments in light of the results in the previous section.

According to the separation approximation[19,32]

$$G(\omega) \approx G_s(\omega) + V_l\,, \tag{17}$$

where G is the Brueckner reaction matrix, and G_s is the reaction matrix due to the "short-range" part of the interaction (V_s). The long-range part of the interaction, V_l, is treated as a perturbation. The "separation" distance (d) is chosen in the Moszkowski-Scott[32] (MS) method such that V_s gives zero phase shift. In the MMS method,[19] the separation distance is chosen such that the defect "reference" wave function, $\chi(\vec{r})$, vanishes for $r \geq d$. In either case, the approximations to the "nuclear" wave functions have the desired "healing" property. The separation distance is usually 1 to 1.5 F.

The reaction matrix, G_s, can be related to the reference spectrum reaction matrix, G_s^R, by means of a Pauli correction term.[19,33] The relation between G_s and G_s^R is given by

$$\langle \vec{k}|G_s(\omega)|\vec{k}'\rangle = \langle \vec{k}|G_s^R(\omega)|\vec{k}'\rangle + \frac{1}{\lambda}\int d^3q \times \frac{\langle \vec{k}|G_s^R(\omega)|\vec{q}\rangle (Q-1)\langle \vec{q}|G_s(\omega)|\vec{k}'\rangle}{\omega - q^2}, \tag{18}$$

where $\lambda = \hbar^2/M$. Since $G_s^R(\omega)$ is determined from the short-range part of the interaction, the reference defect wave function, $\chi_{\vec{q}}(\vec{k})$, which is proportional to $G_s^R(\vec{k}, \vec{q}, \omega)/(\omega - k^2)$, is relatively independent of $\vec{q}$, at least for low and moderate q.[19] Therefore, we may approximate G_s by

$$\langle \vec{k}|G_s(\omega)|\vec{k}'\rangle \approx \langle \vec{k}|G_s^R(\omega)|\vec{k}'\rangle + \frac{1}{\lambda}\langle \vec{k}|G_s^R(\omega)|\vec{k}'\rangle \times \int d^3q \left(\frac{Q-1}{\omega - q^2}\right)\langle \vec{q}|G_s(\omega)|\vec{k}'\rangle. \tag{19}$$

By multiplying both sides of Eq. (19) by $(Q-1)/(\omega - k^2)$ and integrating over k, we may evaluate the integral in Eq. (19) in terms of an integral involving G_s^R. The result, which is also given by BBP, is

$$\langle \vec{k}|G_s(\omega)|\vec{k}'\rangle \approx \langle \vec{k}|G_s^R(\omega)|\vec{k}'\rangle/(1-\eta), \tag{20}$$

where

$$\eta = \frac{1}{\lambda}\int d^3q\,(Q-1)(\omega - q^2)^{-1}\langle \vec{q}|G_s^R(\omega)|\vec{k}'\rangle.$$

From Eq. (20) we obtain, for diagonal G-matrix elements,

$$\langle \vec{k}_0|G(\omega)|\vec{k}_0\rangle \approx \langle \vec{k}_0|G_s^R(\omega)|\vec{k}_0\rangle/(1-\eta) + \langle \vec{k}_0|V_l|\vec{k}_0\rangle. \tag{21}$$

If we further assume that the defect wave function is approximately independent of the starting energy ω, we may rewrite Eq. (21)

$$\langle \vec{k}_0|G(\omega)|\vec{k}_0\rangle \approx S(\vec{k}_0)(\omega - k_0^2) + \langle \vec{k}_0|V_l|\vec{k}_0\rangle, \tag{22}$$

where $S(\vec{k}_0) = \langle \vec{k}_0|G_s^R(\omega)|\vec{k}_0\rangle/[(1-\eta)(\omega - k_0^2)]$ is approximately independent of ω. Apart from the factor $(1-\eta)^{-1}$, $S(\vec{k}_0)$ is the parameter I defined by Coester *et al.*[14] Note that, according to Eq. (22), G is linear in ω. In actual calculations of $G(\omega)$ as a function of ω, we found that G is very nearly linear in ω, at least up to changes in ω of 1 F^{-2}. This change in ω corresponds to a change in the single-particle energies of about 20 MeV. For example, for both the Reid $^1S_0$ potential and potential 2, we calculated the diagonal elements of $G(\omega)$ for several values of ω between $\omega = 2.0$ F^{-2} and $\omega = 3.0$ F^{-2}. We also approximated $G(\omega = 2.0\ \mathrm{F}^{-2})$ by a linear extrapolation from the slope of $G(\omega)$ at $\omega = 3.0$ F^{-2}. The exact values of $G(\omega = 2.0\ \mathrm{F}^{-2})$ disagreed with the extrapolated values by less than 4% of the total change in G. In the $^3S_1 + {}^3D_1$ cases, the agreement ranged from about 90 to 96%. These small errors imply that the ω independence of $S(\vec{k}_0)$ in Eq. (22) is justified. We will later use the near linearity of G in ω to discuss self-consistency corrections.

If we differentiate Eq. (22) with respect to ω, we obtain

$$\frac{\partial}{\partial \omega}\langle \vec{k}_0|G(\omega)|\vec{k}_0\rangle = S(\vec{k}_0). \tag{23}$$

McCarthy and Davies[34] have shown that[35]

$$\frac{\partial}{\partial \omega}\langle \vec{k}_0|G(\omega)|\vec{k}_0\rangle = -\frac{\lambda\kappa}{8\pi^3\rho}. \tag{24}$$

One obtains, from Eqs. (22)–(24),

$$\langle \vec{k}_0|G(\omega)|\vec{k}_0\rangle \approx (k_0^2 - \omega)\lambda\kappa/(8\pi^3\rho) + \langle \vec{k}_0|V_l|\vec{k}_0\rangle. \tag{25}$$

Now we consider two phase-shift equivalent potentials, $\tilde{V}$ and V, with G matrices $\tilde{G}(\omega)$ and $G(\omega)$ and wound integrals $\tilde{\kappa}$ and κ. We assume that Λ is sufficiently short ranged as to leave V_l unaltered. We observe from Eq. (25) that, at a fixed density,

$$\langle \vec{k}_0|\Delta\tilde{G}(\omega)|\vec{k}_0\rangle = (k_0^2 - \omega)\lambda\Delta\tilde{\kappa}/(8\pi^3\rho), \tag{26}$$

where $\Delta\tilde{G} = \tilde{G} - G$, etc. Since ω is negative, we see from Eq. (26) that $\tilde{G}$ becomes more positive for potentials with larger wound integrals. Also, G is linear in κ.

To relate changes in G to changes in binding energies, we employ the relation[35]

$$E - T = \frac{1}{16\pi^3\rho}\sum_{SM_sTT_3}\langle SM_sTT_3|\iint_{k_1,\,k_2 \leq k_F} d^3k_1 d^3k_2 \times \langle \vec{k}_0|G(\omega)|\vec{k}_0\rangle|SM_sTT_3\rangle \tag{27}$$

from which Eq. (11) is derived. In Eq. (27) $\vec{k}_1$ and $\vec{k}_2$ are single-particle momenta and $\vec{k}_0$ is the relative momentum. If we insert Eq. (26) into Eq. (27), with the provision that $\Delta\tilde{\kappa}$ is averaged over spin and isospin quantum numbers, we obtain a

difference in binding energy per particle $\Delta\tilde{E}_0$ given by

$$\Delta\tilde{E}_0 = (\tilde{E}_0 - E) = \frac{\lambda}{8\pi^6\rho^2}\iint_{k_1,\,k_2\le k_F} d^3k_1 d^3k_2 (k_0^2 - \omega)\Delta\tilde{\kappa}\,. \tag{28}$$

Here E is the self-consistent energy per particle for the untransformed (Reid) potential. Of course, $\Delta\tilde{\kappa}$ in Eq. (28) depends on $\vec{k}_0$ and ω. With the assumption that we may replace $\Delta\tilde{\kappa}$ with its average value for two particles in the Fermi sea, one may take $\Delta\tilde{\kappa}$ outside the integrand in Eq. (28). We then employ the fact that the values of ω to be inserted in Eq. (27) are on the "energy shell," i.e.,

$$\begin{aligned}\omega &= k_1^2 + k_2^2 + (1/\lambda)[U(k_1) + U(k_2)] - K^2 \\ &= k_0^2 + (1/\lambda)[U(k_1) + U(k_2)]\,,\end{aligned} \tag{29}$$

where U is the self-consistent single-particle potential energy as determined by the prescription of BBP. Substitution of Eq. (29) into Eq. (28) yields

$$\begin{aligned}\Delta\tilde{E}_0 &= -\frac{\Delta\tilde{\kappa}}{8\pi^6\rho^2}\iint_{k_1,k_2\le k_F} d^3k_1 d^3k_2 [U(k_1) + U(k_2)] \\ &= -\langle U\rangle\Delta\tilde{\kappa}\,,\end{aligned} \tag{30}$$

where $\langle U\rangle$ is the average single-particle potential energy for the untransformed potential V. We finally utilize the relation

$$E - T = \tfrac{1}{2}\langle U\rangle \tag{31}$$

to cast Eq. (30) into the form

$$\Delta\tilde{E}_0 = -2(E - T)\Delta\tilde{\kappa}\,. \tag{32}$$

One must remember that $\tilde{E}_0$ is calculated with an energy spectrum that is self-consistent for the potential V, not for $\tilde{V}$. Therefore, we must correct Eq. (32) to account for a self-consistent energy spectrum for $\tilde{V}$.

In correcting for the changes in ω required by a self-consistent energy spectrum, we assume that G is linear in ω. We then notice that according to Eq. (31), a change in energy $\Delta\tilde{E}_0$ leads to a change in the average potential energy $(\Delta\langle U_0\rangle)$ given by

$$\Delta\langle U_0\rangle = 2\Delta\tilde{E}_0\,. \tag{33}$$

This change in U, in turn, leads to a change in the values of ω to be substituted into Eq. (27). If one employs Eq. (29) to calculate the average change in ω, and Eq. (24) to calculate the change in $\tilde{G}$, substitution into Eq. (27) yields an additional change in $\tilde{E}$ (ΔE_1) of $-\Delta\tilde{E}_1 = -\tilde{\kappa}\langle\Delta U_0\rangle$. This change in energy, likewise, causes a new change in $\langle U\rangle$ for which further corrections are necessary. The final result is an infinite power series in κ that, when summed to all orders, yields[36]

$$\Delta\tilde{E} = \tilde{E} - E = \frac{\Delta\tilde{E}_0}{1 + 2\tilde{\kappa}} = -2(E - T)\Delta\tilde{\kappa}/(1 + 2\tilde{\kappa})\,. \tag{34}$$

Here $\tilde{E}$ is the self-consistent binding energy for the potential $\tilde{V}$. Equation (34) agrees with Brandow's result[17] for self-consistency corrections.

In our computations we calculated $\tilde{E}_0$. We then obtained the approximately self-consistent saturation curves of Figs. 1 and 2 by applying Eq. (34). We found Eq. (34) to be an excellent approximation. In a few test cases, Eq. (34) differed from a self-consistent calculation of $\tilde{E}$ by less than 0.5 MeV, even for large values of $\tilde{\kappa}$ at $k_F = 1.6$ F^{-1}.

Equation (34) tells us that, given the saturation curve for V (in our case the Reid potential), one may construct the saturation curve for the transformed potential $\tilde{V}$. Only the knowledge of κ and $\tilde{\kappa}$ as functions of density is necessary. Since $\Delta\tilde{\kappa}$ is generally an increasing function of density, and since, in the case of the Reid potential, $(T - E)$ is an increasing function of density, then $\Delta\tilde{E}$ is an increasing function of density. Therefore, Eq. (34) accounts for the density dependence of $\Delta\tilde{E}$ observed in Sec. III. The density dependence of $\Delta\tilde{E}$ has a profound effect on the shapes of the saturation curves and the saturation densities.

Equations (32) and (34) qualitatively agree with the results described in Sec. III. For instance, we found that $\tilde{E}_0$ is linear in κ, as predicted by Eq. (32). We also found that $\Delta\tilde{E}$ is an increasing function of density as predicted by Eq. (34); i.e., a larger $\tilde{\kappa}$ yields less binding.

If we analyze Eq. (32) by partial waves, we may rewrite Eq. (32) as

$$\Delta\tilde{E}_0^{\alpha} = -2(E - T)\Delta\tilde{\kappa}^{\alpha}\,, \tag{35}$$

where $\Delta\tilde{E}^{\alpha}$ and $\Delta\tilde{\kappa}^{\alpha}$ are the contributions to $\Delta\tilde{E}_0$ and $\Delta\tilde{\kappa}$ ($\sum_{LL'}\Delta\tilde{\kappa}^{\alpha}_{LL'}$ of Ref. 7) from the partial-wave eigenchannel α. The results in Fig. 4 indicate that, in the $^1S_0$ state, $\Delta\tilde{E}_0^{\alpha}/\Delta\tilde{\kappa}^{\alpha} \approx 78$ MeV for $k_F = 1.6$ F^{-1}. This slope is very close to that predicted by Eq. (35), which is $\Delta\tilde{E}_0/\Delta\tilde{\kappa}^{\alpha}|_{\text{sep.approx.}} \approx 76$ MeV. In Fig. 5, however, for the $^3S_1 + {}^3D_1$ state $\Delta\tilde{E}_0^{\alpha}/\Delta\tilde{\kappa}^{\alpha} \approx 103$ MeV. This slope is significantly larger than that predicted by Eq. (35). In Fig. 6 we compare $\Delta\tilde{E}_0^{\alpha}/\Delta\tilde{\kappa}^{\alpha}$ for both the $^1S_0$ and $^3S_1 + {}^3D_1$ states as obtained from our nuclear matter calculations with $\Delta\tilde{E}_0^{\alpha}/\Delta\tilde{\kappa}^{\alpha}$ predicted by Eq. (35). The $^1S_0$ slopes agree very well with Eq. (35) while the $^3S_1 + {}^3D_1$ slopes are somewhat larger.

The properties of $\Delta\tilde{E}_0^{\alpha}/\Delta\tilde{\kappa}^{\alpha}$ shown in Fig. 6 can be explained as follows. In the $^1S_0$ state V_I is weak and can be treated as a perturbation. Therefore, Eq. (17) should be a good approximation. In the $^3S_1 + {}^3D_1$ state, however, V_I contains a strong tensor force. We expect, therefore, Eq. (17) to be inadequate. We now suggest how Eq. (35) can be

improved for the $^3S_1+{}^3D_1$ state.

We now consider the expression for G through second order in the MMS method, which is, according to BBP,

$$G(\omega)=G_s(\omega)+V_l+2G_s^{\dagger}\frac{Q}{\omega-T}V_l+V_l\frac{Q}{\omega-T}V_l\,. \tag{36}$$

If we rewrite Eq. (36) in integral form and employ Eq. (20) and the boundary conditions on $\chi_{\vec{k}}(\vec{r})$, one obtains the BBP result

$$\begin{aligned}\langle\vec{k}_0|G(\omega)|\vec{k}_0\rangle\approx{}&\langle\vec{k}_0|G_s^R(\omega)|\vec{k}_0\rangle/(1-\eta)+\langle\vec{k}_0|V_l|\vec{k}_0\rangle\\&+(2/\lambda)\int d^3q\,\frac{Q-1}{(\omega-q^2)(1-\eta)}\\&\times\langle\vec{q}|G_s^R(\omega)|\vec{k}_0\rangle\langle\vec{q}|V_l|\vec{k}_0\rangle\\&+(1/\lambda)\int d^3q\langle\vec{k}_0|V_l|\vec{q}\rangle\frac{Q}{\omega-q^2}\langle\vec{q}|V_l|\vec{k}_0\rangle\,.\end{aligned} \tag{37}$$

Employing the Hermiticity of $G_s^R(\omega)$ and the approximate $\vec{q}$ independence of $\chi_{\vec{q}}(\vec{k}_0)$, we rewrite Eq. (37)

$$\begin{aligned}\langle\vec{k}_0|G(\omega)|\vec{k}_0\rangle\approx{}&\langle\vec{k}_0|G_s^R(\omega)|\vec{k}_0\rangle/(1-\eta)[1+(2/\lambda)\eta_1(\omega)]\\&+\langle\vec{k}_0|V_l|\vec{k}_0\rangle+(1/\lambda)\eta_2(\omega)\,,\end{aligned} \tag{38}$$

where

$$\eta_1(\omega)=\int d^3q\left(\frac{Q-1}{\omega-q^2}\right)\langle\vec{q}|V_l|\vec{k}_0\rangle\,,$$

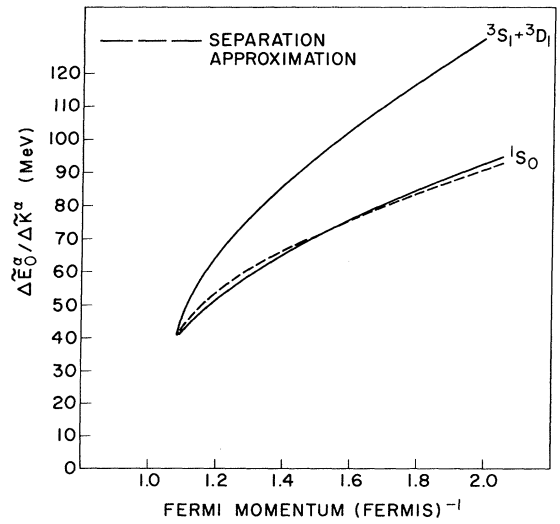

FIG. 6. $\Delta\tilde{E}_0^\alpha/\Delta\tilde{\kappa}^\alpha$ for the $^1S_0$ and $^3S_1+{}^3D_1$ states compared with $\Delta\tilde{E}_0^\alpha/\Delta\tilde{\kappa}^\alpha$ expected from the separation approximation. The slopes $\Delta\tilde{E}_0^\alpha/\Delta\tilde{\kappa}^\alpha$ for the $^1S_0$ and $^3S_1+{}^3D_1$ states are calculated by a "best" linear fit of $\tilde{E}_0^\alpha$ versus $\tilde{\kappa}^\alpha$ for the potentials used in Figs. 1 and 2. The slopes predicted by the separation approximation are given by Eq. (35) and are state independent.

and assume

$$\eta_2(\omega)=\int d^3q\langle\vec{k}_0|V_l|\vec{q}\rangle\left(\frac{Q}{\omega-q^2}\right)\langle\vec{q}|V_l|\vec{k}_0\rangle\,.$$

We now set $S(\vec{k}_0)=\langle\vec{k}_0|G_s^R(\omega)|\vec{k}_0\rangle/[(1-\eta)(\omega-k_0^2)]$ and assume, as before, that $S(\vec{k}_0)$ is independent of ω. We differentiate Eq. (38) with respect to ω and employ Eq. (24). Equation (38) then becomes

$$\begin{aligned}\langle\vec{k}_0|G(\omega)|\vec{k}_0\rangle\approx{}&\left[\frac{\lambda\kappa}{8\pi^3\rho}+\frac{1}{\lambda}\eta_2'(\omega)\right]\\&\times\frac{(k_0^2-\omega)[1+(2/\lambda)\eta_1(\omega)]}{[1+(2/\lambda)\{\eta_1(\omega)+(\omega-k_0^2)\eta_1'(\omega)\}]}\\&+\langle\vec{k}_0|V_l|\vec{k}_0\rangle+(1/\lambda)\eta_2(\omega)\,,\end{aligned} \tag{39}$$

where the primes represent derivatives with respect to ω. The only quantity in Eq. (39) that varies from potential to potential is κ. Note that Eq. (39) is linear in κ although the quantity that multiplies $\lambda\kappa/(8\pi^3\rho)$ is no longer $(k_0^2-\omega)$ as in Eq. (25). In the $^3S_1+{}^3D_1$ state, where $\eta_1'(\omega)$ is large, we expect the coefficient of $\lambda\kappa/(8\pi^3\rho)$ to differ substantially from $(k_0^2-\omega)$.

If Eq. (39) were analyzed by partial waves, and substituted into Eq. (27) to give a binding energy, the result would be of the form

$$\Delta\tilde{E}_0^\alpha\approx C^\alpha(k_F)\Delta\tilde{\kappa}^\alpha\,, \tag{40}$$

where $C^\alpha(k_F)$ depends on k_F, V_l in channel α, and on the self-consistent values of ω for the untransformed potential. The coefficient $C^\alpha(k_F)$ does not depend on the transformed potential $\tilde{V}$.

One could continue our analysis to higher order in G_s and V_l and collect terms linear in κ to derive expression like Eq. (40). In such an analysis, terms of higher order in κ might appear. The results in Figs. 4 and 5 imply, however, that the linear term (40) dominates. The coefficients $C^\alpha(k_F)$ may be empirically determined from the values of $\Delta\tilde{E}_0^\alpha/\Delta\tilde{\kappa}^\alpha$ in Fig. 6.

Equation (40) gives us a very simple prescription for constructing the saturation curves for phase-shift equivalent potentials. Namely, for a given density we have the empirical result

$$\Delta\tilde{E}_0=\sum_\alpha C^\alpha(k_F)\Delta\tilde{\kappa}^\alpha\,, \tag{41}$$

where $C^\alpha(k_F)$ for the $^1S_0$ and the $^3S_1+{}^3D_1$ states is given in Fig. 6. To correct for self-consistency we divide by $1+2\tilde{\kappa}$ to obtain[37]

$$\Delta\tilde{E}=\sum_\alpha C^\alpha(k_F)\Delta\tilde{\kappa}^\alpha/(1+2\tilde{\kappa})\,. \tag{42}$$

Employing the density dependence of $\tilde{\kappa}(^3S_1+{}^3D_1)$ for potentials 10 and 11, we compare in Fig. 7 the saturation curves of these potentials expected from Eq. (42) with those expected from the first-

order separation approximation. We also include the actual saturation curves in Fig. 7. Since forces 10 and 11 were two of the forces used to determine $C^{\alpha}(k_F)$, the curves predicted by Eq. (42) naturally agree well with the actual saturation curves. The saturation curves predicted by the first-order separation approximation give the qualitative features of the actual saturation curves, but fail by several MeV to give the correct binding energies at higher densities. As a further test of the universality of the coefficients $C^{\alpha}(k_F)$, we include the corresponding saturation curves for the Bryan-Scott one-boson-exchange potential (OBEP).[7] Although the Bryan-Scott potential has slightly different bound-state properties, phase-shifts, and long-range behavior than the Reid potential, its saturation curve is qualitatively predicted by Eq. (42) and the separation approximation.

In applying our transformation, we have found that it is difficult, although not impossible, to generate potentials that are smoother (smaller κ) than the untransformed (Reid) potential. However, the consistent linear dependence of $\tilde{E}_0$ and $\tilde{\kappa}$ shown in Figs. 4 and 5 suggests that we may extrapolate our results to smoother potentials. In Fig. 8 we illustrate saturation curves, calculated on the basis of Eq. (42), for five hypothetical functional dependences of $\tilde{\kappa}$ on density. The $^3S_1+{}^3D_1$ wound integrals as functions of density for four of these cases ($H1$–$H4$) appear in Fig. 9. Case $H5$ is a hypothetical case for $\kappa=0$. Case $H4$ has been fit to give the empirical energy per particle (−16 MeV) and saturation density ($k_F \approx 1.4$ F^{-1}). These requirements on $H4$ account for the unusual density dependence of κ. The saturation curves in Fig. 8 suggest that variations in binding energies and saturation densities of up to 12 MeV and 0.24 F^{-1}, respectively, are conceivable for potentials smoother than the Reid potential. These variations are not as large as those reported in Ref. 7. However, the potentials in Ref. 7 were not constrained to give precisely the same fits to the deuteron observables. Potentials corresponding to cases $H1$–$H5$ would be presumably so constrained.

We note that, according to Fig. 8, very smooth potentials overbind nuclear matter and saturate at too high a density. While the saturation curves in Fig. 8 are not the results of actual nuclear matter calculations, they are accurate insofar as Eq. (42) is empirically valid. Furthermore, by virtue of the relatively small values of κ in $H1$–$H5$, the three-body terms of the Goldstone expansion[28,30] should not greatly affect the variations in binding energy.

From the preceding discussion a clear physical picture emerges. Since κ is a measure of the "wound" of the two-nucleon wave function in a nuclear medium, the binding energy of nuclear matter is primarily sensitive to the total "wound." However, the binding energy does not seem to be overly sensitive to the details in the wound, at least up to distances of 1 F.

Considerable interest now exists in formulating nuclear physics in terms of the two-nucleon transition (T) matrix.[20,38] We now demonstrate how

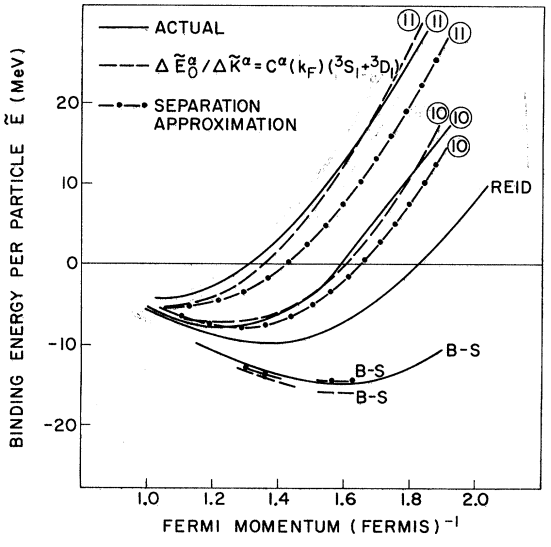

FIG. 7. Actual saturation curves of potentials 10, 11, and the Bryan-Scott (BS) potential compared with those (1) expected from the relation $\Delta\tilde{E}_0^{\alpha}/\Delta\tilde{\kappa}^{\alpha}=C^{\alpha}(k_F)$ and (2) expected from the first-order separation approximation.

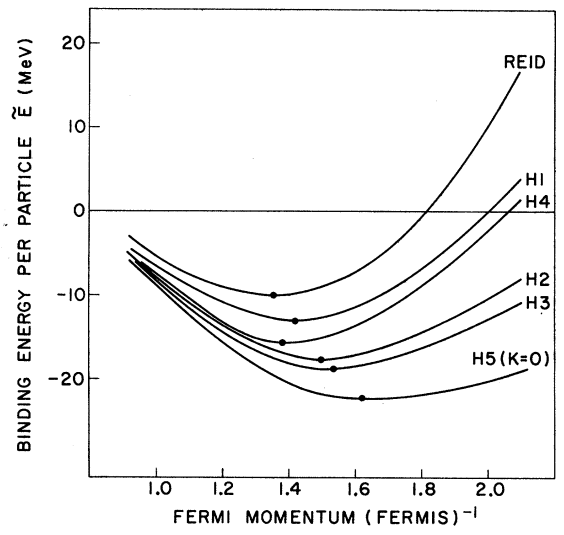

FIG. 8. Saturation curves for five hypothetical cases ($H1$–$H5$). The heavy dots represent saturation minima. Cases ($H1$–$H4$) are defined by Fig. 9. Case $H5$ is for $\kappa=0$.

the sensitivity of nuclear matter to the "wound" of the wave function can be translated to the sensitivity of nuclear matter to the off-shell T matrix. We concentrate our discussion on the so called "half-shell" T matrix. The half-shell T matrix is derivable from the two-nucleon scattering wave functions and, aside from the bound-state wave function, completely determines the off-shell T matrix.

V. NUCLEAR MATTER AND THE T MATRIX

We have found that the binding energy of nuclear matter is determined by κ, the "wound" integral. The wound integral, κ, is determined from the G matrix, not the T matrix. How may we relate the G matrix to the T matrix?

One way to relate G and T is to note that the off-shell T matrix $T(\omega)$ is the same as the reference G matrix $G^R(\omega)$.[33] The G matrix, therefore, is related to the T matrix by a Pauli correction term, which is given in Eq. (18). Since the fully off-shell T matrix, $T(\omega)$, is bilinear in the so-called "half-shell" T matrix,[20,38] the Pauli correction term would involve terms of higher order than two in the half-shell T matrix. While the Pauli corrections are small in the $^1S_0$ case, they are very important in the $^3S_1+{}^3D_1$ state. Therefore an analysis of Eq. (18) in terms of the half-shell T matrix would be fairly complicated.

Our procedure will be to try to correlate binding energies with derivatives of the T matrix. This procedure seems reasonable since κ is proportional to $\partial G/\partial\omega$. Likewise, κ_R, the wound integral of the "reference" wave function, is given by

$$-\frac{\lambda\kappa_R}{8\pi^3\rho}=\frac{\partial}{\partial\omega}\langle\vec{k}_0|T(\omega)|\vec{k}_0\rangle\,. \tag{43}$$

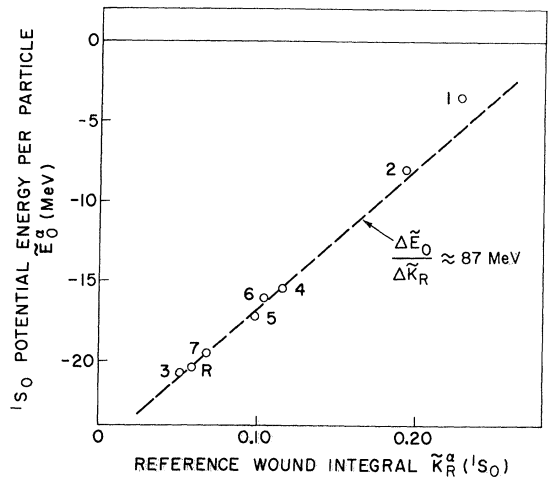

FIG. 10. The $^1S_0$ potential energies $\tilde{E}_0^\alpha$ vs the $^1S_0$ "reference" wound integrals $\tilde{\kappa}_R^\alpha$. The linear relation between $\Delta\tilde{E}_0^\alpha$ and $\Delta\tilde{\kappa}_R^\alpha$ is indicated by a dashed line.

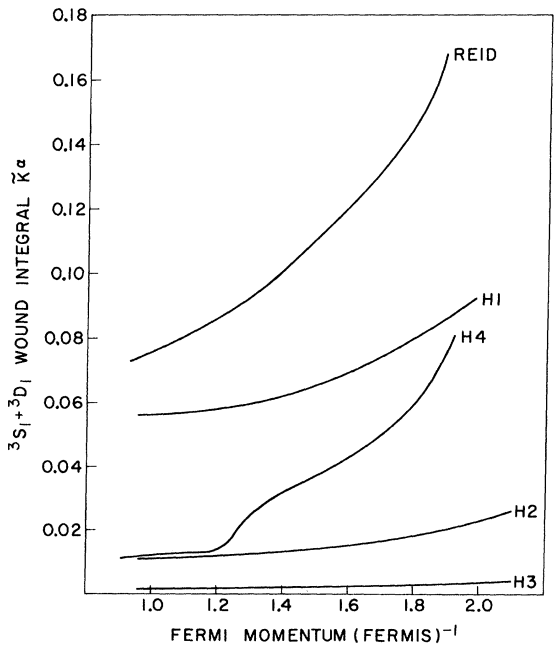

FIG. 9. The $^3S_1+{}^3D_1$ wound integrals, as functions of density, for the Reid potential and hypothetical cases $H1$–$H4$.

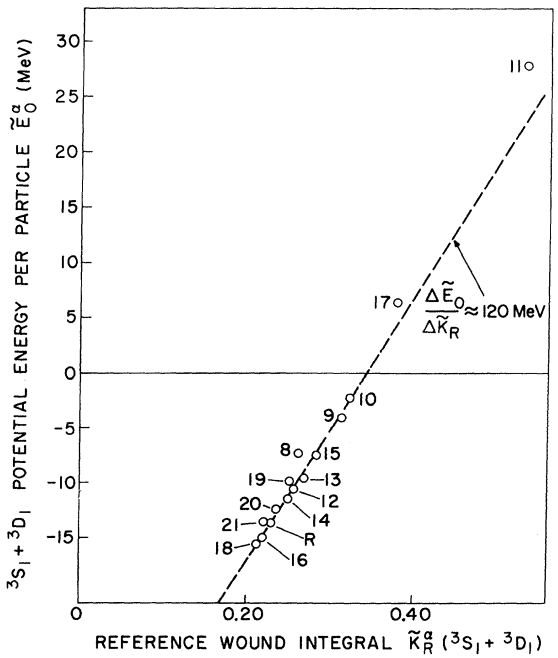

FIG. 11. The $^3S_1+{}^3D_1$ potential energies versus the $^3S_1+{}^3D_1$ "reference" wound integrals $\tilde{\kappa}_R^\alpha$. The linear relation between $\Delta\tilde{E}_0^\alpha$ and $\Delta\tilde{\kappa}_R^\alpha$ is indicated by a dashed line.

In Figs. 10 and 11 we show the binding energies of our transformed potentials versus $\tilde{\kappa}_R^\alpha$ for the $^1S_0$ and $^3S_1+{}^3D_1$ states for $k_F = 1.6$ F^{-1}. In the $^1S_0$ state the correlation between $\tilde{E}_0^\alpha$ and $\tilde{\kappa}_R^\alpha$ is excellent. The binding energies $\tilde{E}_0^\alpha$ are nearly linear in $\tilde{\kappa}_R^\alpha$ with $\Delta\tilde{E}_0^\alpha/\Delta\tilde{\kappa}_R^\alpha \approx 87$ MeV. The slope $\Delta\tilde{E}_0^\alpha/\Delta\tilde{\kappa}_R^\alpha$ is slightly greater than the slope $\Delta\tilde{E}^\alpha/\Delta\tilde{\kappa}^\alpha \approx 78$ MeV. In the $^3S_1+{}^3D_1$ state the correlation is good, although some deviations from linearity occur. The slope $\Delta\tilde{E}^\alpha/\Delta\tilde{\kappa}_R^\alpha \approx 120$ MeV is again greater than the slope $\Delta\tilde{E}^\alpha/\Delta\tilde{\kappa}^\alpha \approx 103$ MeV.

According to the results in Figs. 10 and 11, the binding energy of nuclear matter, at a given density, is correlated with the derivative of the T matrix with respect to energy. The T matrix is determined from the "half-shell" T matrix (denoted by t) by[39]

$$T^\alpha_{LL'}(k,k',\omega) = \sum_l t^\alpha_{Ll}(k,k')[U^T \cos\Delta(k')U]_{lL'} + (2/\pi)\sum_l \int q^2 dq\, t^\alpha_{Ll}(k,q) t_{L'l}(k',q)[1/(\omega - q^2) - P/(k'^2 - q^2)]$$
$$+ [(k'^2 - \omega)(k^2 + k_B{}^2)\omega^\alpha_L(k)\omega^\alpha_{L'}(k')/(\omega + k_B{}^2)]\,, \qquad (44)$$

where P stands for principal value, and $\omega^\alpha_L(k) = \int_0^\infty r^2 dr\, j_L(kr)\omega^\alpha_L(r)$, where $\omega^\alpha_L(r)$ is the $L\alpha$ component of the bound-state wave function with energy $-\lambda k_B{}^2$. In Eq. (44)

$$t^\alpha_{LL'}(k,k') = \sum_l T^\alpha_{Ll}(k,k',k'^2+i\epsilon)[U^T e^{-i\Delta(k')}U]_{lL'}$$

where

$$U = \begin{pmatrix} \cos\epsilon^\alpha & \sin\epsilon^\alpha \\ -\sin\epsilon^\alpha & \cos\epsilon^\alpha \end{pmatrix}, \quad \Delta(k') = \begin{pmatrix} \delta^\alpha_{J-1} & 0 \\ 0 & \delta^\alpha_{J+1}(k') \end{pmatrix}$$

for coupled channels, and $U_{LL'} = \delta_{LL'}$, $\Delta^\alpha_{LL'}(k') = \delta^\alpha_{L'}(k')\delta_{LL'}$ for uncoupled ($L = L'$) channels. The parameters $\delta^\alpha_{LL'}$ and ϵ^α are eigenphase shifts and coupling parameters in the Blatt-Biedenharn parametrization.[40] The matrix elements $T^\alpha_{Ll}(k,k',k'^2+i\epsilon)$ are given by

$$T_{LL'}(k,k',k'^2+i\epsilon) = (1/\lambda)\langle \alpha Lk|V|\Psi^\alpha_{L',k'}\rangle, \qquad (45)$$

where $\langle \vec{r}|\alpha Lk\rangle = j_L(kr)\mathcal{Y}^\alpha_L(\hat{r})$. In Eq. (45) $\Psi^\alpha_{L',k'}$ has the same normalization as $|\alpha Lk\rangle$ and is the contribution to the outgoing solution of the Schrödinger equation for incoming momentum k' and angular momentum L'.

We now consider two potentials V and $\tilde{V}$, with half-shell T matrices t and $\tilde{t}$. Assuming that V and $\tilde{V}$ give approximately the same deuteron wave function, we differentiate Eq. (44) to obtain

$$(\lambda/8\pi^3\rho)\Delta\tilde{\kappa}^\alpha_R \approx (2/\pi)\int_0^\infty q^2 dq\,[\tilde{t}^2(k_0,q) - t^2(k_0,q)] \times (\omega - q^2)^{-2}\,. \qquad (46)$$

In Eq. (46) we have abbreviated $t^2 \equiv \sum_{LL'}(t^\alpha_{LL'})^2$ for coupled channels.

We observe that the squares of t-matrix elements enter into Eq. (46) and that the different components of t^2 ($t_{J-1,J-1}{}^2$, $t_{J-1,J+1}{}^2$, $t_{J+1,J-1}{}^2$, $t_{J+1,J+1}{}^2$) enter with equal coefficients. In an on-shell approximation (i.e., a "phase-shift" approximation) only the central components ($t_{J-1,J-1}$, $t_{J+1,J+1}$) would enter for the binding energy. In Eq. (46) for $\tilde{\kappa}^\alpha_R$, which essentially governs the off-shell variations in binding energies, central and tensor components appear with equal coefficients.

In Fig. 12 we plot, as a function of q, the coefficients $W(q)$ [$W(q) \equiv q^2/(\omega - q^2)^2$] of the t-matrix elements in the integrand of Eq. (46). We choose typical values of k_0 and ω for two particles in the Fermi sea for $k_F = 1.6$ F^{-1}. The weight function, $W(q)$, reaches its maximum value at about $q \approx 1.8$ F^{-1}. At $q \approx 4$ F^{-1}, $W(q)$ is about half of its maximum value; at $q \approx 6$ F^{-1} $W(q)$ is about one quarter of its maximum value. This relatively slow fall-off of $W(q)$ at large q, means that far off-energy-shell matrix elements of t should play a significant role in determining $\Delta\tilde{\kappa}^\alpha_R$.

In Fig. 13 we plot both $\tilde{t}^\alpha(k_0,q)$ as a function of q (the "on-shell" variable), and $\tilde{t}^\alpha(q,k_0)$ as a function of q (the "off-shell" variable) for several transformed $^1S_0$ potentials. We recall that the "on-shell" momentum is the variable integrated over in Eq. (46). We see that, for the potentials considered, $t(q,k_0)$ decreases slowly with q for large values of q. In the case of $t(k_0,q)$, it is not even evident that $t(k_0,q)$ is decreasing in magnitude at $q = 10$ F^{-1}. The properties of $t(k_0,q)$, coupled with the properties of $W(q)$, imply that large contributions to $\Delta\tilde{\kappa}_R$ may come from large values of q ($q \gtrsim 8$ F^{-1}). These large contributions are shown explicitly in Fig. 14.

Figure 14 illustrates the integrand in Eq. (46) [$\Delta(q)$], as a function of q, up to $q = 10$ F^{-1} for potentials 1–4. We notice that for potentials 1, 3, and 4 the largest contribution to $\Delta(q)$ comes from $q \approx 4$ to 10 F^{-1}. For potential 2, the contribution from $q \approx 10$ F^{-1} is especially large. The implication is that far-off-energy-shell matrix elements are important in accounting for changes in $\tilde{\kappa}_R$. These changes in $\tilde{\kappa}_R$ are reflected in changes in $\tilde{\kappa}$ and hence in changes in the binding energy of nuclear matter.

In this section we have observed that changes in binding energy are closely related to changes in

the reference wound integral κ_R. The wound integral κ_R is proportional to $\partial T(\omega)/\partial\omega$, and $\partial T(\omega)/\partial\omega$ is, in turn, bilinear in the "half-shell" T matrix. We thus conclude that the binding energy of nuclear matter is indeed related to the off-shell behavior of the T matrix.

VI. SUMMARY AND DISCUSSION

This paper has shown that off-shell effects in the Brueckner theory of nuclear matter are very significant. Potentials that give the same scattering data and bound-state observables may give variations of up to 9.5 MeV in the binding energy and 0.33 F^{-1} in the saturation density. If we extrapolate our results to smooth potentials, total variations of up to 21 MeV in the binding energy and 0.6 F^{-1} in the saturation density are conceivable.

The principal quantity that governs the energy variations in nuclear matter is the wound integral κ. For a fixed starting energy (ω) and density, the binding energy is nearly linear in κ. This linearity in κ, as shown in Sec. III, simply follows from the MMS separation approximation. The slope $\Delta\tilde{E}_0^\alpha/\Delta\tilde{\kappa}^\alpha$ is greater in the $^3S_1+{}^3D_1$ state than in the $^1S_0$ state. The greater sensitivity of $\Delta\tilde{E}_0^\alpha$ to $\Delta\tilde{\kappa}^\alpha$ in the $^3S_1+{}^3D_1$ state evidentally results from the importance of interference terms between G_s and V_t in the separation approximation. These interference terms are large in the $^3S_1+{}^3D_1$ state due to the strong long-range part of the tensor force.

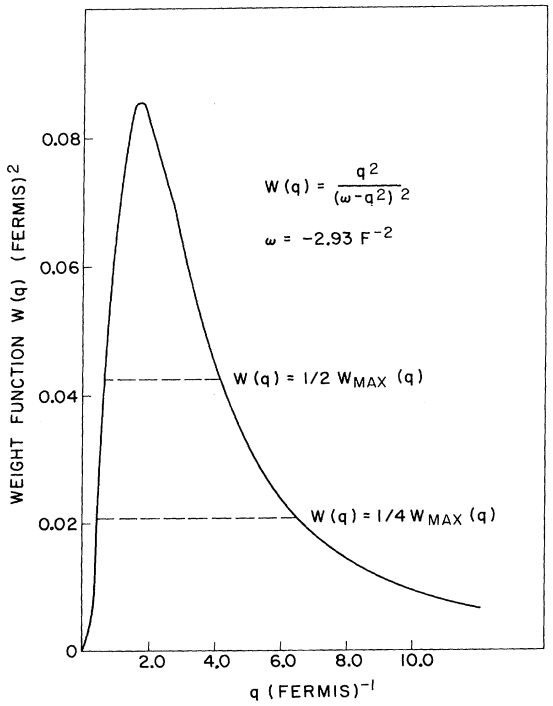

FIG. 12. The "weight" function $W(q)$.

Changes in κ, which lead to changes in binding energy, are closely related to changes in κ_R, the reference spectrum wound integral. The wound integral κ_R, in turn, can be expressed in terms of the half-shell T matrix. By virtue of the values of ω in nuclear matter and the $1/q^2$ behavior of the weight function $W(q)$ at large q, the binding energy of nuclear matter is sensitive to a large region of the off-shell T matrix. The far-off-shell elements ($q \gtrsim 6$ F^{-1}), therefore, play a significant role in nuclear matter.

The principal uncertainty in our calculations is the role of the many-body cluster diagrams in the Goldstone expansion for nuclear matter. Since κ is the accepted expansion parameter for the Goldstone series, one may reasonably expect significant off-shell variations in the many-body terms. These off-shell variations should be sensitive to far-off-shell T-matrix elements because of the sensitivity of κ to these matrix elements. The occupation probability formalism[17, 34, 41] might provide a workable starting point in estimating the off-shell effects in the many-body cluster terms. At any rate, it is unlikely that the inclusion of many-body terms in our calculation (an enormously difficult task) would drastically alter, at least

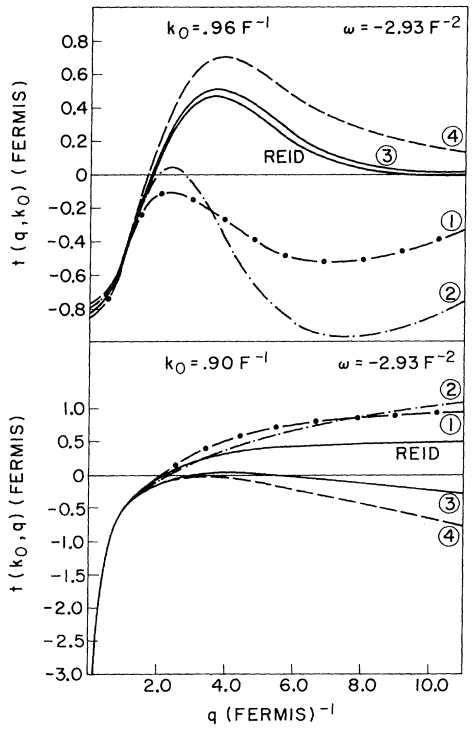

FIG. 13. The "half-shell" T-matrix elements as functions of the "off-" and "on-" shell momenta for the Reid $^1S_0$ potential and the transformed $^1S_0$ potential and the transformed $^1S_0$ potentials 1–4.

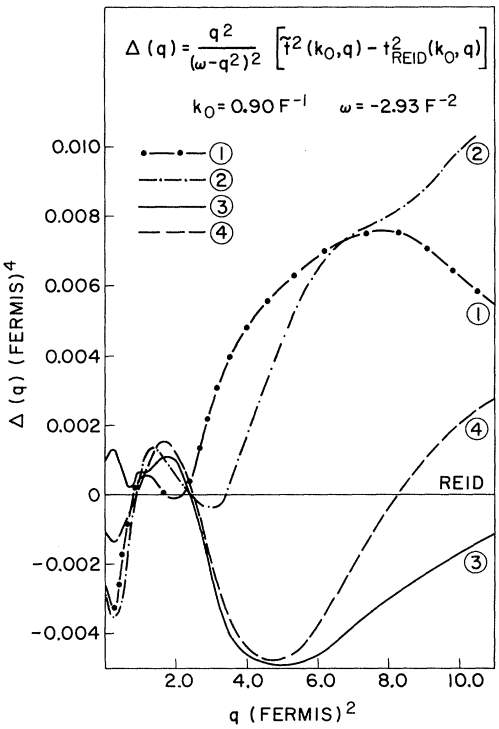

FIG. 14. Contributions to the integrand $[\Delta(q)]$ in expression (46) for $\Delta\bar{r}^{\alpha}_{R}$.

qualitatively, our remarks concerning the sensitivity of nuclear matter to half-shell T-matrix elements. Certainly, extrapolation of our quantitative results is justified to that class of "smooth" potentials ($\kappa \lesssim \kappa_{\mathrm{Reid}}$) for which many-body contributions should be small.

The potentials studied in this paper give variations in κ of about three times the value of κ for the Reid potential. This variation in κ is larger than the variation in κ of Ref. 14 and considerably larger than the variation in Ref. 7. For equal changes in $\kappa^{\alpha}(^1S_0)$ we get variations in binding energy comparable to those of Coester *et al.* We do not, however, get in the $^3S_1 + {}^3D_1$ state as large variation in binding energy for like changes in κ as those reported in Ref. 7. One must remember, however, that the potentials in Ref. 7 were not constrained to give exactly the same phase shifts, long-range behavior, or the same electric form factor as the Reid potential. In fact, these latter three constraints probably account for about 8 of the 22-MeV difference in binding between the Reid potential and force "A" of Ref. 7. The point here is that one should apply empirical constraints on the deuteron wave function and meson-theoretic constraints on the long-range part of the potential before attributing variations in binding energy to off-shell effects.

The linear dependence of the energy per particle on κ holds only for potentials with approximately the same electric form factors. The electric form factor, however, does not uniquely determine the binding-energy result. We have observed that potentials with almost exactly the same $F_{el}(q)$ can give drastically different wound integrals and binding energies. It therefore follows that even with the requirement of a precision fit to the experimental values of deuteron form factor, it would still be possible to have potentials that give very different binding energies in nuclear matter. For example, the Reid potential and potential 11 give almost exactly the same deuteron wave function yet give binding energies that differ by 9.5 MeV.

The results of this paper imply that even with the presently available empirical and theoretic constraints on the N-N interaction, a major ambiguity still exists with respect to off-shell matrix elements. Since nuclear matter is sensitive to a large region of the off-shell T matrix, nuclear matter calculations should play an important role in resolving the ambiguities. Nuclear matter calculations should be used in conjunction with calculations of other processes, such as the p-$2p$ knockout reactions,[42] to help clarify the role of both near and far-off-energy shell matrix elements. Until the roles of the off-shell matrix elements is resolved, a meaningful comparison between theory and experiment of the properties of nuclei is very difficult.

ACKNOWLEDGMENTS

We would like to thank Dr. F. Coester for several conversations and for suggesting his transformation to us before publication. We are grateful to Dr. C. M. Vincent for critically reading the manuscript and for his helpful comments. One of us (M.I.H.) would like to thank Dr. E. F. Redish for helpful conversations. He would also like to thank Dr. Mervine Rosen for his help in the deuteron form-factor calculation.

---

*National Research Council – Naval Research Laboratory Postdoctoral Resident Research Associate.

[1]R. A. Bryan and B. L. Scott, Phys. Rev. 135, B434 (1964); 164, 1215 (1967); 177, 1435 (1969).

[2]A. E. S. Green and T. Sawada, Rev. Mod. Phys. 39, 594 (1967); T. Ueda and A. E. S. Green, Phys. Rev. 174,

1350 (1968).

[3]F. Coester, to be published.

[4]L. Ingber, Phys. Rev. 174, 1250 (1968).

[5]D. W. Sprung, in *Proceedings of the Third International Conference on Atomic Masses and Related Constants, Winnipeg, Canada, 1967,* edited by R. C. Barber (University of Manitoba Press, Winnipeg, Canada, 1968).

[6]A. Kallio and B. D. Day, Nucl. Phys. A124, 177 (1969).

[7]M. Haftel, Ph.D. thesis, University of Pittsburgh, 1969 (unpublished); M. Haftel and F. Tabakin, Nucl. Phys. A158, 1 (1970).

[8]P. V. Siemens, Nucl. Phys. A141, 225 (1970).

[9]A. H. Cromer and M. I. Sobel, Phys. Rev. 152, 1351 (1966).

[10]V. R. Brown, Phys. Rev. 177, 1498 (1969).

[11]F. J. D. Serduke and I. R. Afnan, Bull. Am. Phys. Soc. 15, 65 (1970).

[12]T. Brady, E. Harms, L. Laroze, and J. S. Levinger, Phys. Rev. C 2, 59 (1970).

[13]M. D. Miller, M. S. Sher, P. Signell, and N. R. Yoder Phys. Letters 30B, 157 (1969); E. Lomon, Bull. Am. Phys. Soc. 14, 493 (1969); M. K. Srivastava, P. K. Banerjee, and D. W. L. Sprung, Phys. Letters 31B, 499 (1970).

[14]F. Coester, S. Cohen, B. Day, and C. M. Vincent, Phys. Rev. C 1, 769 (1970).

[15]R. V. Reid, Ann. Phys. (N.Y.) 50, 411 (1968).

[16]M. A. Preston and R. K. Bhaduri, Can. J. Phys. 42, 696 (1964).

[17]B. H. Brandow, Phys. Rev. 152, 863 (1966).

[18]B. H. Brandow, Rev. Mod. Phys. 39, 771 (1967).

[19]H. A. Bethe, B. H. Brandow, and A. G. Petschek, Phys. Rev. 129, 225 (1963). We will refer to this paper as BBP.

[20]M. Baranger, B. Giraud, S. K. Mukhopadhyay, and P. U. Sauer, Nucl. Phys. A138, 1 (1969).

[21]H. Ekstein, Phys. Rev. 117, 1590 (1960).

[22]G. A. Baker, Phys. Rev. 128, 1485 (1962).

[23]K. A. Brueckner, C. A. Levinson, and H. M. Mahmoud, Phys. Rev. 95, 217 (1954); and K. A. Brueckner and K. S. Masterson, Jr., *ibid.* 128, 2267 (1962).

[24]P. C. Bhargava and D. W. L. Sprung, Ann. Phys. (N.Y.) 42, 222 (1967).

[25]Our definition of $F_{el}{}^2(q^2)$ corresponds to the quantity $G_{Ed}{}^2 + \frac{8}{9}\eta^2 G_{Qd}{}^2$ given by D. Benaksas, D. Drickey, and D. Frerejacque, Phys. Rev. 148, 1327 (1966).

[26]J. E. Elias, J. I. Friedman, G. C. Hartmann, H. W. Kendall, P. N. Kirk, M. R. Sogard, and L. P. Van Speybroeck, Phys. Rev. 177, 2075 (1969). Other references listed here.

[27]The test we apply is whether a transformed potential gives the same form factor as the Reid soft-core potential. While we do not compare the form factors directly with experiment, we use the experimental percentage errors to classify the transformed potentials. According to Ref. 26, the Reid potential gives a satisfactory fit to the experimental deuteron electric form factor. Investigations of the role of the deuteron form factor are being conducted by H. A. Bethe, private communication.

[28]For general real θ, (except $\theta = n\pi/2$) it is possible to generate a tensor force in $\tilde{V}$ even if V has no tensor component. For $\sin\theta$ equal to 0 or 1, this possibility does not exist.

[29]R. Rajaraman and H. A. Bethe, Rev. Mod. Phys. 39, 745 (1967) and other references listed here.

[30]P. A. Lawson, Nucl. Phys. A143, 65 (1970).

[31]J. Goldstone, Proc. Roy. Soc. (London) A239, 267 (1957).

[32]S. A. Moszkowski and B. L. Scott, Ann. Phys. (N.Y.) 11, 65 (1960).

[33]M. Baranger, in *Proceedings of the International School of Physics "Enrico Fermi," Course XL, Varenna, 1967* (Academic Press Inc., New York, 1969).

[34]R. J. McCarthy and K. T. R. Davies, Phys. Rev. C 1, 1644 (1970).

[35]Actually, we should be dealing with antisymmetrized G-martix elements, i.e., $\langle \vec{k} | G(\omega) | \vec{k}' \rangle \rightarrow \langle \mu\nu | G(\omega) | \mu'\nu' - \nu'\mu' \rangle$, where particles in the single-particle states μ and ν have relative momentum $\vec{k}$, and the particles in states μ' and ν' have relative momentum $\vec{k}'$. With this understanding, Eq. (24) is compatible with Eq. (16) and Eq. (27) gives the binding energy.

[36]A similar result was obtained by C. W. Wong on the basis of the separation approximation. Wong's result was $\Delta E \approx -\frac{3}{4}\langle U \rangle \Delta\kappa$. C. W. Wong, Nucl. Phys. 56, 213 (1964); 71, 385 (1965).

[37]Despite the somewhat complicated ω dependence in Eq. (39), we found the linear approximation satisfactory.

[38]M. I. Haftel, Phys. Rev. Letters 25, 120 (1970).

[39]Equation (44) is essentially the relation between T and t given in Refs. 20 and 38. The relation has been generalized to include coupled partial waves.

[40]J. M. Blatt and L. C. Biedenharn, Phys. Rev. 86, 399 (1952).

[41]M. Baranger and M. Johnson, to be published.

[42]E. F. Redish, G. J. Stephenson, Jr., and G. M. Lerner, Center for Theoretical Physics, University of Maryland Technical Report No. 70-120, 1970 (unpublished); E. F. Redish, private communication. The p-$2p$ knockout reaction may be sensitive to half-shell T-matrix elements that are off the energy shell by as much as 1.5 F^{-1}.